Available online at www.sciencedirect.com

ScienceDirect

journal homepage: www.elsevier.com/locate/he

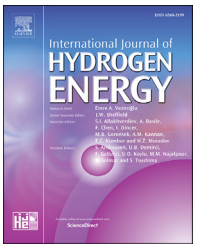

Effect of glidants on $LaNi_5$ powder flowability

Maximiliano Melnichuk [a,b,*], *Diego J. Cuscueta* [a,c], *Nicolas Silin* [a,c]

[a] *CONICET: Consejo Nacional de Investigaciones Científicas y Técnicas, Centro Atómico Bariloche (C.N.E.A), Av. E. Bustillo 9500, CP 8400, S.C. de Bariloche, Río Negro, Argentina*

[b] *C.N.E.A.: Comisión Nacional de Energía Atómica, Centro Atómico Bariloche, Av. E. Bustillo 9500, CP 8400, S.C. de Bariloche, Río Negro, Argentina*

[c] *INSTITUTO BALSEIRO, Centro Atómico Bariloche (C.N.E.A.), Universidad Nacional de Cuyo, Av. E. Bustillo 9500, CP 8400, S.C. de Bariloche, Río Negro, Argentina*

ARTICLE INFO

Article history:
Received 17 November 2017
Received in revised form
24 January 2018
Accepted 30 January 2018
Available online 2 March 2018

Keywords:
$LaNi_5$ hydride flowability
Rotating drum
Glidant agents
Hydride container tension accumulation

ABSTRACT

Tension accumulation in container walls is a matter of concern in hydride based hydrogen storage systems. As the hydrogen absorbing material swells during hydrogen absorption it will need to flow and accommodate within its container. Failure to do so will result in the build-up of tensions and, eventually, in the failure of the container after a number of absorption-desorption cycles. There have been several ways of avoiding the build-up of mechanical stresses: having a container geometry that allows the swelling of the hydride, combining the hydride forming alloys with other materials that can handle the volume increase or the stresses, and adding solid lubricants to improve the ability of the hydride to accommodate within the container. In the present study we explore the application of nanoscaled powders normally used in the industry as glidant agents for bulk powders. In particular, we address the influence of three different types of glidants in the flowability of $LaNi_5$ powder: Aerosil R 805, molybdenum disulfide (MoS_2) and Vulcan XC72 carbon black. For this purpose, we have used a pressurized rotating drum device that allows hydrogen pressure or vacuum to test $LaNi_5$ in hydrogen absorbed or desorbed states. The angle of repose results indicate an improvement on powder flowability when using Aerosil in concentrations of approximately 0.05 wt% or MoS_2 at concentrations of approximately 0.1 wt%. These results are in agreement with models that explain the reduction of inter-particle forces when using small quantities of nanoscaled particles. Vulcan XC72 showed no effectiveness as glidant. This unexpected behavior is most likely related to its tendency to become trapped in the cracks of the larger $LaNi_5$ particles and to form relatively large aggregates.

Introduction

Hydrogen storage by means of hydride forming alloys is a technology field under development. These materials offer the opportunity to store hydrogen, while avoiding high pressure compression or cryogenic liquefaction needed in other storage solutions, both energy demanding processes. A suitable hydrogen storage material has to fulfil a series of characteristics: high volumetric and gravimetric storage capacity, equilibrium conditions near ambient pressure and temperature, fast reaction rate, high cyclability, etc. In addition to

* *Corresponding author*. Centro Atómico Bariloche (C.N.E.A.), Av. Bustillo 9500, CP 8400, S. C. de Bariloche, Rio Negro, Argentina.
E-mail address: mmelnichuk@cab.cnea.gov.ar (M. Melnichuk).

https://doi.org/10.1016/j.ijhydene.2018.01.207

these characteristics, related to physico-chemical properties of the material, there are engineering aspects that must be addressed in order to use hydride forming alloys in large scales: cost [1–4], heat management [5,6], hydrogen flow [7] and the containment of the micrometric hydrogen storage material [8]. One of these engineering aspects is how to deal with the swelling of the storage material powder during the absorption process. This is not a minor issue as hydride forming alloys can vary their volume up to approximately 20% during hydrogen absorption [9].

When a hydride forming alloy undergoes swelling and shrinking cycles, two related phenomena commonly occur: the reduction of the alloy powder, and the rise of tensions in the walls of the container [8,10–12]. These two processes are interconnected as the fines produced during the absorption-desorption cycles tend to percolate to the lowest areas increasing the packing ratio and the tensions produced [13]. Some studies show that tension keeps building up even after plastic deformation of the containment vessel [14], while other studies report higher tension values during activation of the hydride [15,16]. Changes in alloy powder itself have been reported due to tension accumulation, reducing particle size and compacting the powder [17,18]. Particularly, it has been proposed that one powder reduction mechanism is originated in the friction between the particles [19].

One approach to avoid the build-up of tensions in the container walls is to allow the material to flow and accommodate as it swells during hydrogen absorption [20] in a rigid container, failure to do so will result in tension accumulation in the walls and, eventually, in mechanical failure. Tension accumulation is, therefore, largely dependent on interparticle friction [21] and, more generally, on the flowability of the hydrogen absorbing material. The ability of fine powders to flow is hindered by the action of van der Waals forces, which become dominant as the particle size decreases [22–24]. This is the case for hydrogen absorbing materials, as particle size distribution ranges from 10^{-1} μm–10^{2} μm [25].

There have been previous attempts to mitigate the accumulation of tensions due to hydride swelling by incorporating solid lubricants or elastomers. Baker and Lynch incorporate such materials in fractions of about 10% in weight or 30% in volume reducing densification, compaction and stress build-up during cycling [26]. They used fluorocarbon materials to enhance flowability, such as DuPont Teflon 7A and Viton, in particle sizes of the same range as hydride particles. Their material choice also considered the chemical compatibility with the hydride forming alloy.

Another approach involved manufacturing composite materials based on a hydrogen absorbing alloy and a second material capable of coupling with the swelling of the alloy. Heubner et al. describe the testing of a composite consisting of a primary hydrogen absorbing phase and conclude they can achieve very high volumetric storage densities [27]. Blytas details the use of a plastic elastomer binder in a concentration between 2 and 15 wt% to form pellets with $LaNi_5$. These pellets show good mechanical characteristics while maintaining hydrogen capacity [28]. Sometimes this second material may also have high thermal conductivity thus also improving the absorption dynamics [29–31]. This approach is successful in eliminating tensions in the container walls, but in some cases the degradation of the material could not be avoided [17,32].

In 1974, Rumpf showed that increased surface roughness leads to a reduction of interparticle forces for originally smooth particles [33,34]. Surface roughness works by increasing the distance between the primary surfaces of two interacting particles. The particles of materials used as glidants are characterized by diameters in the lower nanometer range. In consequence, they are strongly adsorbed on the surfaces of larger particles and act in the same manner as surface roughness, i.e. they work as spacers between the surfaces of the primary particles. This leads to a reduction of the total contact area between the particles. As a result the van der Waals forces are reduced allowing gravitational or other forces to prevail. From various literature sources it is known that an amount of glidant ranging from 0 to 1 vol % greatly improves the flow of bulk powders [22,35].

According to Meyer and Zimmermann [34], the capacity of a nanomaterial to act as glidant is almost independent of its chemical nature. However, the size of nanomaterials as well as their tendency to agglomerate do depend on the composition and/or the manufacturing method. On the other hand, it is of utmost importance that the chosen glidant does not react with the hydrogen absorbing material as this could hinder its capacity. These aspects make the chemical nature of the glidant important.

In a previous work, we studied the flowability of $LaNi_5$, a well-known hydrogen storage material, by means of a modified rotating drum that allows testing under different hydrogen pressures [36]. Among conclusions, an evaluation regarding how flowability is affected when using different amounts of glidants was suggested. The method of the rotating drum allowed us to determine the interparticle friction variation of the hydride forming alloy as a function of activation and hydrogen charge. In a recent work, Charlas et al. [21] used rotating drum measurements to calibrate a Discrete Element Modelling (DEM) numerical model that was then applied to calculate strains and stresses in a hydride container subject to cycling.

In the present work, we study the effect of adding nano-scaled glidant agents to activated $LaNi_5$ on the angle of repose and the density of the powder, both in charged and discharged states. As glidant candidates, we have chosen Aerosil R 805, a well-established glidant agent, and Vulcan XC72 carbon black. We have also tested MoS_2 which is a well-established solid lubricant with a significant fraction of particles smaller than 1 μm.

Experimental method

Material preparation

To obtain the hydrogen storage material $LaNi_5$, pure elements were melted in an arc furnace under argon, then turned and re-melted five times to improve homogeneity. Once cooled, the alloy ingots were crushed and sieved to obtain a particle size range from 74 μm to 1410 μm.

Activation was performed in a stainless steel reactor with the following characteristics: 16 mm external diameter,

12 mm internal diameter and 140 mm length. The reactor was immersed in a thermostatic water bath at room temperature. According to previous estimations of reaction time for this set-up [6], we performed an absorption of 22 min at 20 bar of high purity hydrogen (5.0), and a desorption of 28 min against mechanical pump vacuum. After 14 cycles under these conditions, the resulting material was sieved in a glove box with a 70 μm sieve, discarding larger particles.

Considering the requirement of chemical neutrality for glidants, our first choice was Aerosil R 805, a nanometric silica powder widely used for this purpose. We also performed tests using carbon black powder, trade name Vulcan XC72 from Cabot. Another glidant we tested is Molybdenum disulfide (MoS_2) from Molykote which, in spite of having sulphur in its composition, is not suspected of contaminating the hydride powder. According to an early study by Eckert [37], MoS_2 in a pure hydrogen atmosphere presents a significant decomposition only when above 715 °C. There have been numerous studies on the poisoning of hydrides, but they are limited to highly reactive gases, such as SH_2 [38–40]. In case the MoS_2 interacts with the hydrogen absorbing material, we expect such interaction to be only superficial [41].

Materials handling and mixing

All handling of the absorbing material after activation was made under controlled atmosphere in a M-Braun MB10 glove box (oxygen concentration $\leq$ 4 ppm/vol and humidity concentration $\leq$ 2 ppm/vol). The weight of both the absorbing material and the flowing agents was measured using a Radwag AS 220 R2 analytic scale inside the glove box. The mixture of the flowing agents and the absorbing material was first performed by hand shaking using a volumetric flask, and then by rolling the rotating drum, at least, 100 turns. We compared the angle of repose distribution of a sample mixed by this method with the same sample mixed 1500 turns more, without noticing any measurable difference, which indicates that mixing time may not play a role under the conditions of the present study.

In the case of Aerosil, it was necessary to gently break agglomerates inside a beaker before mixing it with $LaNi_5$ powder until no agglomerates could be recognized by the naked eye. According to Majerová et al. [22], the primary particles of the glidants exist in the form of agglomerates which are broken down into smaller aggregates during the blending process. These smaller aggregates adsorb at the surface of the other solid component particles and thus diminish attractive van der Waals forces by increasing the roughness of the host surface.

It is worth noting that handling difficulties are consistent with the dynamic angle of repose results: for those mixtures that showed higher angle of repose during rotating drum tests, indicating a more cohesive behavior, we observed ratholes and stable arches while using a funnel inside the globe box.

Experimental set-up and image processing

A rotating drum capable of withstanding 12 bar pressure was used during the present study. The rotating drum cavity has a diameter of (50.0 ± 0.5) mm and a depth of (15.0 ± 0.5) mm. The cylindrical wall was sandblasted to maximize friction while a thick float glass was used on both sides to have optical access and minimize friction. The angular velocity was set to (4.2 ± 0.1) rpm.

To inject or extract hydrogen, a 0.5 μm nominal passage stainless steel filter was fitted flush with the cylindrical wall. A matt green surface was placed behind the rear glass to enhance imaging contrast (Fig. 1). Measurements were performed with a fixed volume of approximately 8 cm^3 of uncompacted powder.

To measure the angle of repose, we obtained videos at 60 frames per second with a Nikon 1 J5 camera. Among the information obtained after processing the videos, we show the mean upper angle of repose (β) before an avalanche event occurs, with its respective standard deviation (error bar). We consider the upper angle of repose to be the most meaningful parameter to address the powder flowability. Every result is obtained from averaging a minimum of 150 upper angle measurements. More details of image capture and processing can be found in Ref. [36]. Density evolution was addressed by calculating the hydride volume from the videos and weighting the material inside the drum after each experiment.

Particle size measurements

Since flowability is strongly influenced by particle size and particle size distribution [42], we measured the particle size distribution of $LaNi_5$ and MoS_2 by means of a Mastersize 3000 particle size analyzer. For this purpose, samples of the powders were retrieved and dispersed in deionized water. The results of the size analysis are shown in Fig. 2.

The use of water as dispersant could lead to the deterioration of the hydrogen absorbing material that could result in changes in particle size distribution. To verify the size distribution results, hydride powder samples were carefully dispersed on graphite adherent substrate to obtain SEM images with an FEI Inspect S50 microscope (Fig. 3). In the case of slender particles, we measured both the major and the minor axis. To address the particle size distribution, we calculated the Dv10, Dv50 and Dv90 parameters which are the threshold sizes corresponding to the 10%, 50% and 90% cumulative

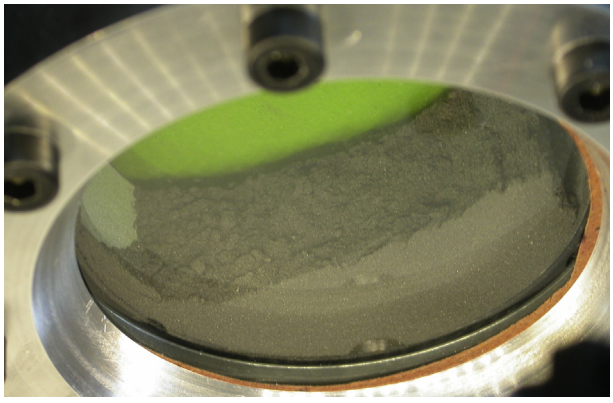

Fig. 1 – Picture of the rotating drum with an activated $LaNi_5$ sample inside.

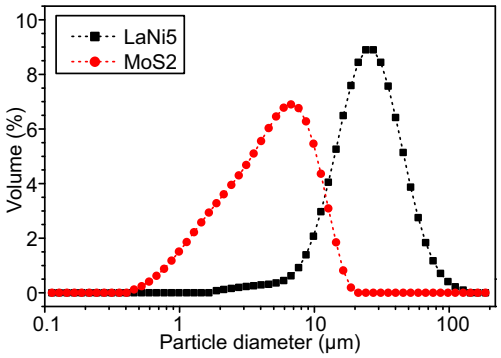

Fig. 2 – $LaNi_5$ and MoS_2 particle size distribution.

volume. After measuring more than 1100 particles from a number of SEM images, we obtained a particle size distribution that closely matched Fig. 2, with a Dv50 of 21 μm. On the other hand, the Dv50 parameter obtained with the particle size analyzer was 27.6 μm, showing good agreement.

Due to experimental conditions, which involved high purity hydrogen or argon atmosphere at all times, liquid bridge type interparticle forces are not expected. Therefore, the main interparticle force is presumed to be of van der Waals type.

The van der Waals attraction force (F_{vdW}) between two particles separated by a smaller spacer particle, schematically shown in Fig. 4, can be calculated following the equation presented by Zimmermann et al. [43].

$$F_{vdW} = -A/6\left[rR/\left(e^2(r+R)\right) + R/\left(32(r+e)^2\right)\right] \quad (1)$$

where A is the Hamaker constant of the particles, r the spacer particle radius, R the powder particle radius and e the distance between them (see Fig. 4).

Here, the Hamaker constant depends on the material involved, being 6.5×10^{-20} J for silica [44] and $\approx 25 \times 10^{-20}$ J for graphite [45]. If we estimate the forces for our $LaNi_5$ particle distribution according to eq. (1), assuming silicon particles as spacers and an interparticle distance e of 0.4 nm [43], we obtain the results shown in Fig. 5.

From Fig. 5, we can estimate that an effective spacer particle will have a radius of 10 nm or more. According to this model, particles larger than 10 nm in radius will produce nearly the same effect regardless of their size. It is also noted that even though the value of the Hamaker constant for spacer particles of different materials does change, this has a minor effect on the resulting force as long as the spacer particle has a radius close to 10 nm. In our case, both Aerosil R 805 and Vulcan XC72 have a primary particle size in this order of magnitude [42,46].

Aerosil particles are originally found in an aggregated state and it is required that these aggregates undergo a degradation process so that individual particles become available as glidant elements. This can be achieved either by long mixing times or by the application of very high shear forces [42]. In our case, neither of these methods could be implemented with the metal hydride, therefore we have to assume that glidant agents are not present in the form of primary particles but as particle aggregates. The mixing that we performed after each glidant agent addition was carried out at low rotation speeds only to achieve a homogeneous distribution of the glidant in the mixture.

The second material tested is not a glidant but rather a solid lubricant, molybdenum disulfide powder (MoS_2). The particle size distribution of MoS_2 was obtained by means of the particle size analyzer (Fig. 2) with particle sizes extending into the submicron range. This material shows low chemical reactivity and it is widely used as a solid lubricant. It has a layered structure held together by weak van der Waals forces and can be mechanically exfoliated to produce flakes that work as a lubricant.

The last glidant candidate that we analyzed is Vulcan XC72 carbon black. Carbon blacks can work effectively as glidant agents though they can behave very differently depending on the morphology of their aggregates. As thermal management is an important aspect of hydride based hydrogen container design [6,47], we opted for Vulcan XC72. This type of carbon black has been successfully used to increase the thermal conductivity of materials, and one of its distinctive features is the formation of long and branched aggregates [48]. According to Liu et al., carbon black primary particles are fused together via covalent bonds to form aggregates [49]. Therefore, the aggregate represents the true smallest structural unit of carbon black, yet it is not clear from theoretical considerations (Fig. 5) how the larger aggregate size will affect flowability.

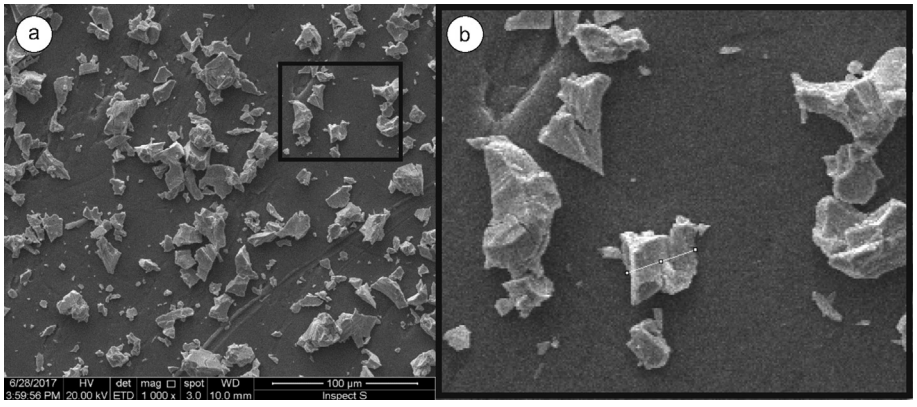

Fig. 3 – SEM images for $LaNi_5$ particle size measurement. a) General picture, b) Detail of single particle measurement.

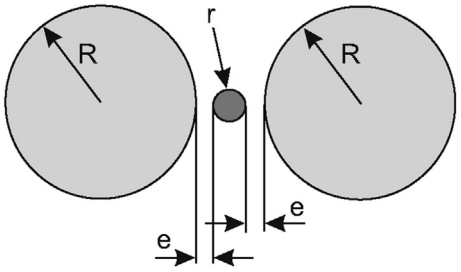

Fig. 4 – Interparticle model with a smaller glidant particle attached to the main particle.

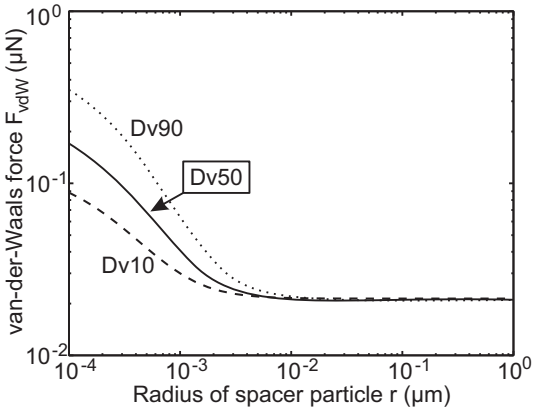

Fig. 5 – Calculated adhesive force as a function of actual powder particle size.

In Table 1, we present the main physical properties of the three glidant candidates and of the $LaNi_5$. The measurement of primary particles of nanometer sized powders is a challenging task as these particles are not found individually but as part of strong aggregates [52]. In this work, we observed the nanometer sized glidants by TEM microscopy (Philips CM200 UT) to estimate the primary particle sizes. We also observed that these powders formed aggregates involving similar sized particles, therefore, it was difficult to achieve a good statistical convergence in the size estimation. For this reason, the particle sizes reported for Aerosil R 805 and Vulcan XC72 should be regarded as an approximate value.

Results and discussion

The avalanche angle and relative density for activated $LaNi_5$ as a function of Aerosil weight ratio are shown in Fig. 6, for

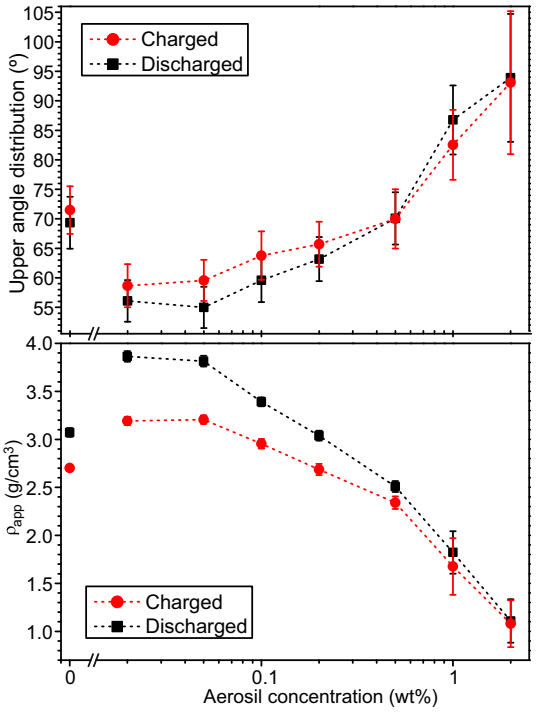

Fig. 6 – Influence of Aerosil glidant on $LaNi_5$ upper angle of repose and bulk density.

both charged (hydrogen concentration at maximum absorption capacity) and discharged states (absorbing material depleted from hydrogen). Charging and discharging processes take place in the rotating drum, while the addition of the glidants requires the opening of the rotating drum in a glove box under controlled atmosphere. As in our previous work [36], we observed a smaller angle of repose for the discharged state. In general, the measurements show better flowability and higher relative density near 0.1 wt% glidant concentration. This tendency is in accordance with previous results [22,43], and the improvement in flowability is consistent with the increase in packing capacity [53–55].

For concentrations of Aerosil above 0.5 wt%, the density change between the charged and discharged states, becomes relatively small. This might occur since overall density becomes much lower when Aerosil is used with these concentrations. On the other hand, the use of glidant above 1 wt% is strongly detrimental to flowability, causing higher angles of repose than those measured for $LaNi_5$ with no glidant added, with median values even above 90°. From present results, we consider that it is not relevant to determine the angle of repose for mixtures with this glidant for concentrations above 2 wt%.

Table 1 – Physical properties of the three glidants and of $LaNi_5$ powder.

Commercial name	Composition	Density	Particle size
Aerosil R805	Silica (amorphous)	2.2 g cm^{-3} [46]	20 to 75 nm
Molikote Z	MoS_2 (cristaline)	5.06 g cm^{-3} [50]	Dv10 = 1.5 μm, Dv50 = 5.1 μm, Dv90 = 11 μm
Vulcan XC72	Graphite (amorphous)	2.04 g cm^{-3} [51]	9 to 80 nm
–	$LaNi_5$ (cristaline)	8.31 g cm^{-3} [6]	Dv10 = 13 μm Dv50 = 28 μm, Dv90 = 60 μm

It is worth considering that our results are quite similar to those obtained by Majerová et al. [22] or Zimmermann et al. [43], who determined a maximum bulk density for binary mixtures of maize starch with ≈0.2 wt% Aerosil.

The avalanche angle and relative density for activated $LaNi_5$ are shown in Fig. 7 as a function of MoS_2 concentration for charged and discharged states. We can observe an initial decrease of avalanche angle, indicating improved flowability with lubricant concentration in the 0.1 wt% vicinity. MoS_2 is not usually used as glidant for powders but it is incorporated as a lubricant in different applications. As lubricant concentration increases, we observe an increase of the avalanche angle to values similar to the case with no lubricant added, indicating that the optimum lubricant concentration have been exceeded. In Fig. 7, we can also observe that the decrease of the avalanche angle correlates with an increase in the powder apparent density.

We performed a test using 5 wt% of MoS_2, obtaining angles of repose similar to those for the 2 wt% case. From direct observation of the powder mixture in the rotating drum, we note that as powder becomes more cohesive it eventually slides as a block, leading to a coexistence of an avalanche with a movement as a solid, resulting in lower angles of repose. This implies that MoS_2 concentration results above 1 wt% may not be representative of flowability variation.

The last glidant candidate we studied is carbon black (Vulcan XC72). It has been used as powder glidant and has good thermal conductivity. It is also not expected to react with the hydride forming alloy. Avalanche angle and relative density for activated $LaNi_5$ as a function of carbon black concentration are shown in Fig. 8. We could not observe any concentration that would lead to an improved powder flowability for this glidant candidate. This behavior differs from previous studies using other types of carbon black such as Printex 95 [43]. When handling Vulcan XC72, the high cohesivity of the powder also becomes apparent, requiring to sieve this material and mix it with a spatula to obtain a satisfactory dispersion in the hydride. Present results suggest that Vulcan XC72 is not a satisfactory glidant candidate for $LaNi_5$ at any concentration.

The flowability decrease for concentrations above 1 wt% for both MoS_2 and Aerosil, is consistent with previous observations of glidants behavior [35]. An accepted model states that for low glidant concentrations, the adhesive force is reduced as the small glidant particles increase the spacing between larger particles, but as glidant concentration increases, a saturation of the surface of the host particle occurs and glidant interparticle adhesion becomes relevant. This, in turn, decreases the flowability of the powder [35]. This phenomenon is schematically shown in Fig. 9.

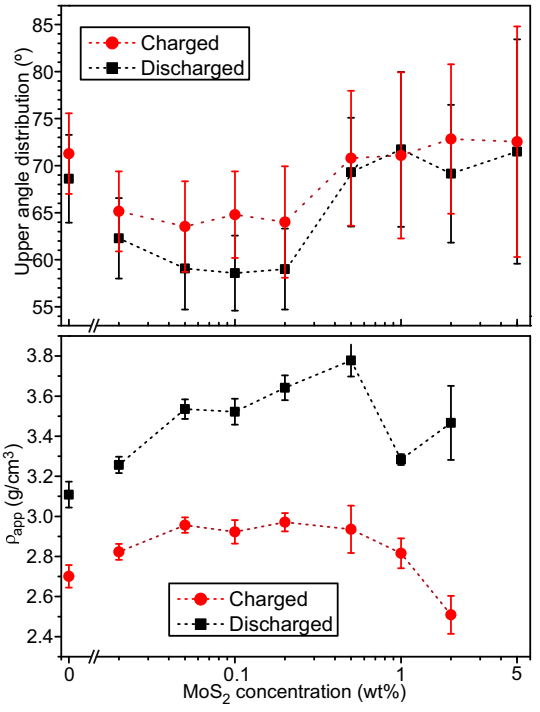

Fig. 7 – Influence of MoS_2 glidant on $LaNi_5$ upper angle of repose and bulk density.

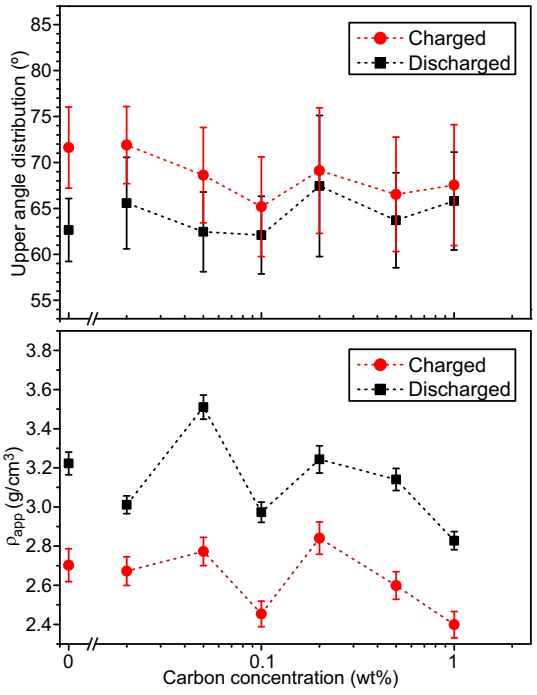

Fig. 8 – Influence of carbon black glidant on $LaNi_5$ upper angle of repose and bulk density.

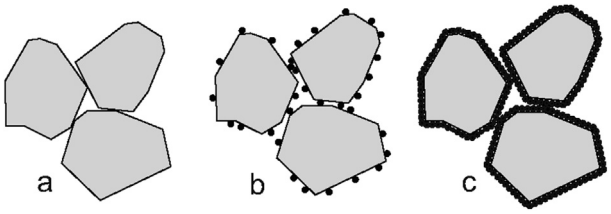

Fig. 9 – Schematic distribution of glidant on host particles: a) no glidant, b) low glidant concentration, c) high (saturated) glidant concentration.

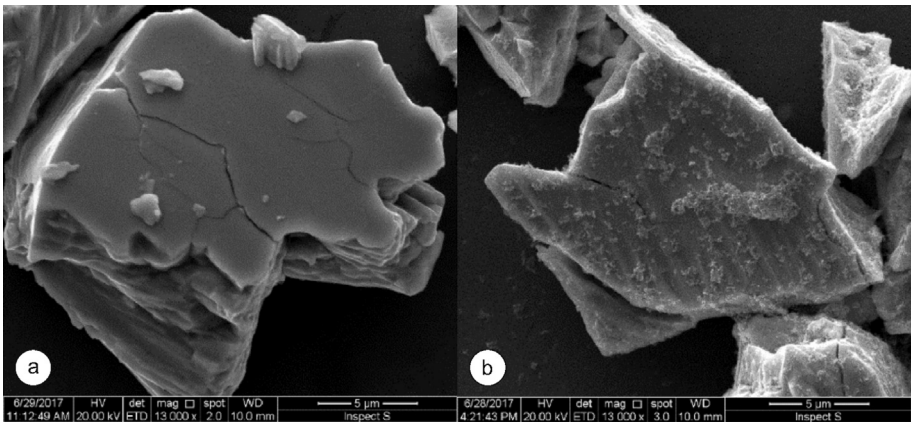

Fig. 10 – SEM images of a) a single $LaNi_5$ particle and b) a single $LaNi_5$ particle with 0.2 wt% Aerosil.

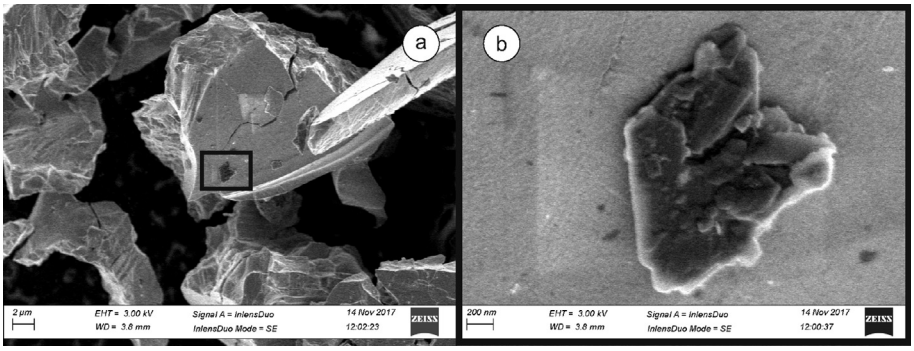

Fig. 11 – SEM images of a) $LaNi_5$ particles with adsorbed MoS_2 submicronic particles (0.2 wt%) and b) detail of MoS_2 particle on the surface of a $LaNi_5$ particle.

Moreover, previous efforts to mitigate mechanical issues described in US Patents 4,600,525 and 4,036,944 can also be interpreted from Fig. 9c). The authors used fluorocarbon or elastomer materials in concentration in the ≈10 wt% range, observing lesser tension accumulation in the container walls as hydride swelled during absorption. We understand this result as the consequence of using a material with better flowing capacity than bulk hydride in a concentration which allows it to be a continuum medium, thus leading to better flowability. We consider that the present results are based on a different mechanism, illustrated in Fig. 9b), and therefore are complementary to the approach used in the mentioned patents.

To gain better insight into the behavior of the different glidant candidates, we have inspected samples of activated $LaNi_5$ with 0.2 wt% of glidant by means of SEM images (FEI

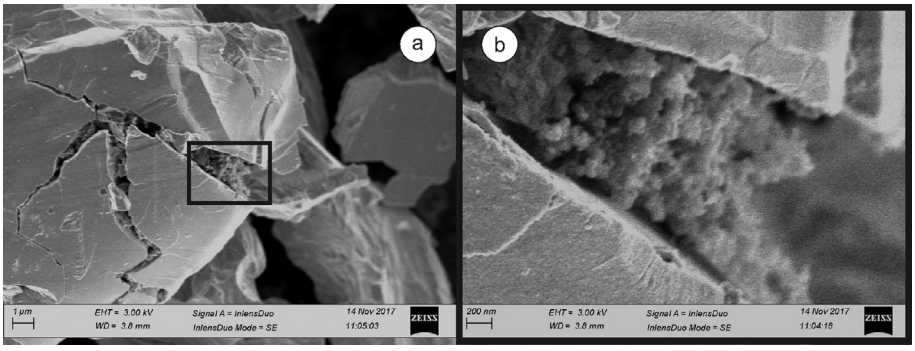

Fig. 12 – SEM images of a) $LaNi_5$ particles with Vulcan XC72 carbon black submicronic particles (0.1 wt%) b) detail of carbon black particles retained in cracks of $LaNi_5$ particles.

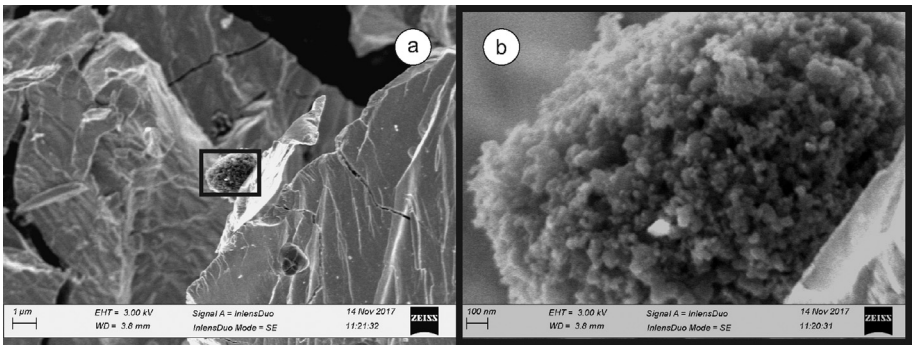

Fig. 13 – SEM images of a) $LaNi_5$ particles with Vulcan XC72 carbon black aggregated particles (0.1 wt%) b) detail of carbon black aggregate.

Inspect S50 and Zeiss Cross Beam 340 microscopes). The samples were taken from the rotating drum after the corresponding test was carried out. In Fig. 10a) we can see an image of the original $LaNi_5$ powder and in Fig. 10b) a mixture of the $LaNi_5$ sample with 0.2 wt% Aerosil. We can observe there are small agglomerates evenly distributed on the surface of the $LaNi_5$ particles. This image is in agreement with the conceptual model of Fig. 9b), showing higher roughness of a $LaNi_5$ particle when compared with a particle with no glidant.

In Fig. 11, we see the image of $LaNi_5$ particles with adsorbed MoS_2 particles on the surface. MoS_2 particles are an order of magnitude larger than Aerosil primary particles and cover a smaller portion of the surface of the hydride. This observation suggests a less effective performance as a flowing agent, which is consistent with angles of repose shown in Figs. 6 and 7.

In Fig. 12, we observe the image of $LaNi_5$ particles with Vulcan XC72 carbon black with a concentration of 0.1 wt%. In this case, most of the glidant particles have been retained in the cracks of the hydride, while the surface of the particle shows no signs of glidant presence. We have also identified some glidant that was not retained in cracks but the particles were found forming tight aggregates in all cases, as shown in Fig. 13. This means that carbon black particles do not become dispersed on the surface of $LaNi_5$, as it is the case of the other glidant candidates, which is consistent with the results showing its ineffectiveness as glidant in our experimental conditions. The reasons for this might be related to a higher Hamaker constant than that of silica, in addition to larger and stronger particle aggregates.

Conclusions

We determined a flowability improvement of activated $LaNi_5$ powder as a function of glidant concentration using a modified rotating drum, for both charged and discharged states. We tested three glidant candidates: Aerosil R 805, MoS_2 and Vulcan XC72 carbon black. Aerosil and MoS_2 powder showed a similar behavior with best performances for concentrations of $\approx$0.05 wt% and $\approx$0.1 wt% respectively. Concentrations above 1 wt% eliminated the beneficial effect on flowability, leading to higher angles of repose that indicate a more cohesive behavior. Apparent density evolution is consistent with angle of repose results, showing better packing capacity at glidant concentrations with lower angle of repose.

The effect of added Vulcan XC72 carbon black as glidant was unsatisfactory. When inspected by means of SEM images, it became apparent that carbon black becomes retained in the cracks of $LaNi_5$ or lumped in aggregates. This behavior causes the particles to be unavailable on the surface of the hydride, therefore ineffective as glidant.

Further work needs to be done to confirm that flowability improvement by means of small quantities of glidant agents shall decrease tension accumulation in the container walls during absorption process.

Acknowledgments

Authors want to thank Dr. E. Lima for his contribution in particle size determination of glidants, Dr. M. Soldati for TEM images, Mr. B. Pentke, Dr. A. Baruj and Ms. P. Troyon for SEM images, and Mr J. Villacura for $LaNi_5$ melting. Dr. M. Melnichuk wants to thank Prof. Frank Lynch for valuable comments on US Patents related to flow aid materials. The present work was financially supported by the following Argentinean institutions: CNEA, Conicet and ANCyT (project codes PICT-1510-2012 and PIP 0535).

REFERENCES

[1] Neelis M, van der Kooi H, Geerlings J. Exergetic life cycle analysis of hydrogen production and storage systems for automotive applications. Int J Hydrogen Energy 2004;29:537–45.

[2] Eigen N, Keller C, Dornheim M, Klassen T, Bormann R. Industrial production of light metal hydrides for hydrogen storage. Scripta Mater 2007;56:847–51.

[3] Pfeifer P, Wall C, Jensen O, Hahn H, Fichtner M. Thermal coupling of a high temperature PEM fuel cell with a complex hydride tank. Int J Hydrogen Energy 2009;43:3457–66.

[4] Lasher S, McKenney K, Sinha J, Chin O. Analyses of hydrogen storage materials and on-board systems. DOE Merit Review 2009. Web site: https://energy.gov/sites/prod/files/2014/03/f12/deliv_analysis_lasher.pdf (Dic 2017).

[5] Pasini JM, Corgnale C, van Hassel BA, Motyka T, Kumar S, Simmons KL. Metal hydride material requirements for automotive hydrogen storage systems. Int J Hydrogen Energy 2013;38(23):9755–65.
[6] Melnichuk M, Silin N. Guidelines for thermal management design of hydride containers. Int J Hydrogen Energy 2012;37(23):18080–94.
[7] Chaise A, Marty P, De Rango P, Fruchart D. A simple criterion for estimating the effect of pressure gradients during hydrogen absorption in a hydride reactor. Int J Heat Mass Tran 2009;52(19):4564–72.
[8] Escobar AG, Chaise A, Iosub V, Salque B, Fernandez JF, Gillia O. Stress effect on the swelling/shrinking behavior of an AB_2 alloy during hydrogenation cycles. Int J Hydrogen Energy 2017;42(35):22422–31.
[9] Matsushita M, Monde M, Mitsutake Y. Experimental formula for estimating porosity in a metal hydride packed bed. Int J Hydrogen Energy 2013;38(17):7056–64.
[10] Charlas B, Chaise A, Gillia O, Doremus P, Imbault D. Investigation of hydride powder bed swelling and shrinking during hydrogen absorption/desorption cycles under different compressive stresses. J Alloy Comp 2013;580:149–52.
[11] Verga M, Armanasco F, Guardamagna G, Valli C, Bianchin A, Agresti F, et al. Scaling up effect of Mg hydride in a temperature and pressure-controlled hydrogen storage device. Int J Hydrogen Energy 2009;34:4602–10.
[12] Ao BY, Chen SX, Jian GQ. A study on wall stresses induced by $LaNi_5$ alloy hydrogen absorption-desorption cycles. J Alloy Comp 2005;390:122–6.
[13] Okumura M, Terui K, Ikado A, Saito Y, Shoji M, Matsushita Y, et al. Investigation of wall stress development and packing ratio distribution in the metal hydride reactor. Int J Hydrogen Energy 2012;37(8):6686–93.
[14] Nasako K, Ito Y, Hiro N, Osumi M. Stress on a reaction vessel by the swelling of a hydrogen absorbing alloy. J Alloy Comp 1998;264(1):271–6.
[15] Duan W, Du J, Wang Z, Niu Y, Huang T, Li Z, et al. Strain variation on the reaction tank of high hydrogen content during hydrogen absorption-desorption cycles. Int J Hydrogen Energy 2013;38(5):2347–51.
[16] Salque B, Chaise A, Iosub V, Gillia O, Charlas B, Dupuis C, et al. Measure of the hydride breathing while cyclically absorbing and desorbing hydrogen. J Alloy Comp 2015;645:S353–6.
[17] Gattia DM, Montone A, Di Sarcina I, Nacucchi M, De Pascalis F, Re M, et al. On the degradation mechanisms of Mg hydride pellets for hydrogen storage in tanks. Int J Hydrogen Energy 2016;41(23):9834–40.
[18] Ham B, Junkaew A, Arróyave R, Park J, Zhou HC, Foley D, et al. Size and stress dependent hydrogen desorption in metastable Mg hydride films. Int J Hydrogen Energy 2014;39(6):2597–607.
[19] Okumura M, Ikado A, Saito Y, Aoki H, Miura T, Kawakami Y. Pulverization mechanism of hydrogen storage alloys on microscale packing structure. Int J Hydrogen Energy 2012;37(14):10715–23.
[20] McKillip T, Banister C, Clark E. Stress analysis of hydride vessels used for tritium storage. Fusion Technol 1992;21:1011.
[21] Charlas B, Kneib F, Gillia O, Imbault D, Doremus P. A tool for modelling the breathing of hydride powder in its container while cyclically absorbing and desorbing hydrogen. Int J Hydrogen Energy 2015;40:2283–94.
[22] Majerová D, Kulaviak L, Ruzicka M, Stepánek F, Zámostny P. Effect of colloidal silica on rheological properties of common pharmaceutical excipients. Eur J Pharm Biopharm 2016;106:2–8.
[23] Visser J. Van der Waals and other cohesive forces affecting powder fluidization. Powder Technol 1989;58:1–10.
[24] Seville JPK, Willett CD, Knight PC. Inter-particle forces in fluidization: a review. Powder Technol 2000;113:261–8.
[25] Hahne E, Kalleweit J. Thermal conductivity of metal hydride materials for storage of hydrogen: experimental investigations. Int J Hydrogen Energy 1998;23:107–14.
[26] Baker NR, Lynch FE. U.S. Patent 4,600,525-Hydrogen sorbent flow aid composition and containment thereof. 1986.
[27] Heubner F, Pohlmann C, Mauermann S, Kieback B, Röntzsch L. Mechanical stresses originating from metal hydride composites during cyclic hydrogenation. Int J Hydrogen Energy 2015;40(32):10123–30.
[28] Blytas GC. (Shell Oil Company) U. S. Patent 4,036,944-Hydrogen sorbent composition and its use. 1977.
[29] Kim KJ, Montoya B, Razani A, Lee K-H. Metal hydride compacts of improved thermal conductivity. Int J Hydrogen Energy 2001;26:609–13.
[30] Pohlmann C, Röntzsch L, Weibgärber T, Kieback B. Heat and gas transport properties in pelletized hydride-graphite-composites for hydrogen storage applications. Int J Hydrogen Energy 2013;38:1685–91.
[31] Chaise A, de Rango P, Marty P, Fruchart D, Miraglia S, Olives R, et al. Enhancement of hydrogen sorption in magnesium hydride using expanded natural graphite. Int J Hydrogen Energy 2009;34:8589–96.
[32] Khandelwal A, Agresti F, Capurso G, Lo Russo S, Maddalena A, Gialanella S, et al. Int J Hydrogen Energy 2010;35:3565–71.
[33] Rumpf H. Die Wissenschaft des Agglomerierens. Chemie-Ingenieur-Technik 1974;46:1–11.
[34] Meyer K, Zimmermann I. Effect of glidants in binary powder mixtures. Powder Technol 2004;139:40–54.
[35] Schulze D. In: Powders and bulk solids – behavior, characterization, storage and flow. Springer; 2008. p. 211–5. ISBN 978-3-540-73767-4.
[36] Melnichuk M, Cuscueta DJ, Silin N. $LaNi_5$ hydride powder flowability as a function of activation and hydrogen content. Int J Hydrogen Energy 2017;42:15799–807.
[37] Eckert G. Beständigkeit von molybdändisulfid gegenüber gasen bei höheren temperaturen. Mater Corros 1958;9:69–72.
[38] Corré S, Gotoh Y, Sakaguchi H, Fruchart D, Adachi G-Y. The hydrogen confinement in $LaNi_5$ and $LaNi_5Zr_{0.1}$ hydrides using poisonous gases. J Alloy Comp 1997;225:117–21.
[39] Schweppe F, Martin M, Fromm E. Hydrogen absorption of $LaNi_5$ powders precovered with O_2, CO, H_2S, CO_2 or N_2. J Alloy Comp 1997;253–254:511–4.
[40] Sandrock GD, Goodell PD. Cyclic life of metal hydrides with impure hydrogen: overview and engineering considerations. J Less Common Met 1984;104:159–73.
[41] Myhra S, Kisi EH, Gray EM. A surface analytical study of SO_2 stabilitation of $LaNi_5H_x$ surfaces. J Alloy Comp 1995;224:305–15.
[42] Huang Z, Scicolone JV, Han X, Davé RN. Improved blend and tablet properties of fine pharmaceutical powders via dry particle coating. Int J Pharm 2015;478:447–55.
[43] Zimmermann I, Eber M, Meyer K. Nanomaterials as flow regulators in dry powders. Z J Phys Chem 2004;218:51–102.
[44] Bergstrom L. Hamaker constants of inorganic materials. Adv Colloid Interface Sci 1997;70:125–69.
[45] Li J-L, Chun J, Wingreen NS, Car R, Askay I, Saville DA. Use of dielectric functions in the theory of dispersion forces. Phys Rev B 2005;71. 235412.
[46] Technical overview Aerosil ® Evonik. Nov 2017. Web site: https://www.aerosil.com/sites/lists/RE/DocumentsSI/Technical-Overview-AEROSIL-Fumed-Silica-EN.pdf.
[47] Melnichuk M, Silin N, Peretti HA. Optimized heat transfer fin design for a metal-hydride hydrogen storage container. Int J Hydrogen Energy 2009;34:3417–24.

[48] Wang J, Li Q, Wu C, Xu H. Thermal conductivity and mechanical properties of carbon black filled silicone rubber. Polym Polym Compos 2014;22:393–9.
[49] Liu ZY, Zhang JL, Yu PT, Zhang JX, Makharia R, More KL, et al. Transmission electron microscopy observation of corrosion behaviors of platinized carbon blacks under thermal and electrochemical conditions. J Electrochem Soc 2010;157:906–13.
[50] Haynes WM, editor. CRC handbook of chemistry and physics. 92nd ed. Boca Raton, FL: CRC Press; 2011. ISBN 1439855110.
[51] Alcántara R, Jiménez-Mateos JM, Lavela P, Tirado JL. Carbon black: a promising electrode material for sodium-ion batteries. Electrochem Commun 2001;3(11):639–42.
[52] Batz-Sohn CH. Particle size of fumed silica: a virtual model to describe fractal aggregates. In: Organo-silicon chemistry VI: from molecules to materials (2 Volumes) by Norbert Auner and Johann Weis. KGaA, Weinheim: WILEY-VCHVerlag GmbH & Co; 2005.
[53] Abdullah EC, Geldart D. The use of bulk density measurements as flowability indicators. Powder Technol 1999;102:151–65.
[54] Carr RL. Evaluating flow properties of solids. Chem Eng 1965;72:163–8.
[55] Pirard S, Lumay G, Vandewalle N, Pirard J-P. Motion of carbon nanotubes in a rotating drum: the dynamic angle of repose and a bed behavior diagram. J Chem Eng 2009;146:143–7.